IEEE Access
Multidisciplinary | Rapid Review | Open Access Journal

Received February 1, 2020, accepted February 17, 2020, date of publication March 6, 2020, date of current version March 17, 2020.

Digital Object Identifier 10.1109/ACCESS.2020.2978916

Suppressing the Capacitor Voltage Fluctuations in Low Frequency Operation of Modular Multilevel Converters

MUNEER AL SABBAGH[1], (Member, IEEE), HABIBUR REHMAN[2], (Member, IEEE), JIANYU PAN[1], (Member, IEEE), AND LONGYA XU[1], (Fellow, IEEE)

[1]Department of Electrical and Computer Engineering, The Ohio State University, Columbus, OH 43210, USA
[2]Department of Electrical Engineering, American University of Sharjah, Sharjah, UAE

Corresponding author: Muneer Al Sabbagh (alsabbagh.2@osu.edu)

This work was supported by the U.S. Department of Energy under Grant DE-EE0007255.

ABSTRACT Low frequency operation in the modular multilevel converters (MMCs) is enabled by applying a reference common mode voltage and circulating currents at a frequency much higher than the desired output frequency. The frequency of injected common-mode signals is limited for maintaining a good performance in the circulating current control. Firstly, this paper theoretically analyzes the effect of increasing the frequency of injected common-mode signals by evaluating the error between reference and actual circulating currents. Secondly, we introduce an additional parameter in the reference circulating current to enhance the suppression of MMC's capacitor voltage fluctuations. Intensive computer simulations are developed for a seven-level MMC driving a medium-voltage induction motor drive system to verify the circulating current error analysis and assess the capacitor voltage fluctuations. Finally, the proposed technique for suppressing the capacitor voltage fluctuations is experimentally validated on a 600-V three-level MMC feeding an inductive load. The voltage fluctuations are reduced by more than 50% (63.6%) when the proposed technique is applied with a high common-mode frequency.

INDEX TERMS Modular multilevel converter, variable speed drive, low frequency operation, circulating current control.

I. INTRODUCTION

Driven by its scalability, small footprint and low harmonic distortion, the modular multilevel converter (MMC) [1], [2] has become an attractive choice for medium-voltage drive applications [3], [4]. However, the capacitor voltage fluctuations in low-speed operation is one of the biggest challenges in MMC-based variable speed drives. These fluctuations are found to be inversely proportional to the output frequency [5]. Therefore, the problem of capacitor voltage fluctuations becomes more severe at low frequency operation of the MMC. As a solution to this problem, a sinusoidal common-mode voltage and circulating currents are injected at a frequency much higher than the AC output frequency [6]. In this way, energy imbalance between the upper and lower arms in one phase is suppressed, resulting in stabilized submodule voltages while applying low-frequency voltages to the motor. Also, it has been pointed out that submodule voltage fluctuations are inversely proportional to the common-mode frequency [6].

Recently several modifications to this technique have been proposed [7]–[12]. Some of these techniques include changing the shape of the injected voltage [7], determining the required circulating current in real-time [8], or performing the control in the $\alpha - \beta$ coordinates [9]. Others suggest using open-loop circulating current control [10], adding a third harmonic of the common-mode frequency to circulating currents [11], or reducing the circulating current levels [12]. Theoretical analyses of all of these techniques [6]–[12] assume that the circulating current follows its command without any deviation. Furthermore, low common-mode frequencies (< 200 Hz) compared to carrier and sampling frequencies are utilized to enable satisfactory current control performance. A detailed review of these common-mode injection techniques can be found in [13].

Two parameters, the capacitor size and common-mode frequency, determine the extent of voltage fluctuations in the submodules when the common-mode injection technique is

The associate editor coordinating the review of this manuscript and approving it for publication was Tariq Masood.

applied with sufficient accuracy. Both parameters have an inverse relationship with the voltage fluctuations. That is, the voltage fluctuations become smaller as the submodule capacitance or the common-mode frequency gets larger, and vice versa. It is desired to increase the power density in the MMC. Therefore, it is prudent to use high common-mode frequencies to reduce the size of submodule capacitors. However, an increase in frequency may cause errors in the circulating currents, and these errors result in undesired voltage fluctuations in the submodules at the output frequency [14]. In our earlier work, a technique to mitigate these voltage fluctuations due to the error has been proposed [14]. The proposed technique improves the suppression of capacitor voltages at a low output frequency by compensating the circulating current error using two parameters α^* (amplitude compensation) and θ^* (phase compensation). These two new parameters are applied in the reference signal and their values are determined by trial and error. However, selecting two parameters is not an easy procedure due to the available large range of selection.

To simplify the technique proposed in [14], we proved in [15] that the same objective can be achieved by only one additional parameter in the circulating current reference instead of two. As a result, the proposed technique becomes simpler, and is able to enhance the suppression of voltage fluctuations in the MMC capacitors.

This paper is based on our earlier work presented in [14] and [15] with the following additional contributions: (i) The reasons for circulating current errors are explained when the common-mode frequency increases. (ii) A method for computing the circulating current error is introduced and a clear relationship between the error and the compensation parameter is established. (iii) Improvements in suppressing the voltage fluctuations are analyzed and validated in the time and frequency domains. (iv) Computer simulations for a medium-voltage MMC drive are performed instead of a low-voltage drive [14], [15]. (v) Experimental results showing a comparison of the old and proposed techniques are added in this paper.

The rest of the paper is organized as follows: Section II presents the MMC system overview and the existing common-mode injection technique. Section III focuses on the analysis of circulating current errors. The proposed technique is described in Section IV. Simulation and experimental results are shown in Section V and VI, respectively. Finally, concluding remarks highlighting the contributions made by this work can be found in Section VII of this paper.

II. MMC SYSTEM OVERVIEW AND INJECTION METHOD

A typical modular multilevel converter (MMC) supplied by a dc voltage V_{dc} feeding a three-phase AC load is shown in Fig. 1. The converter consists of three phase legs denoted by subscripts "a", "b" and "c". Each leg is made of an upper and lower arm, which are indicated by subscripts "p" and "n", respectively. In each arm N half-bridge submodules are stacked in series with an inductor L_{arm}. The upper and lower arm inductors are mutually coupled to provide current-limiting capability to the circulating currents through the legs while giving nearly zero inductance in the load current loop. The basic MMC principles of operation can be found in [4].

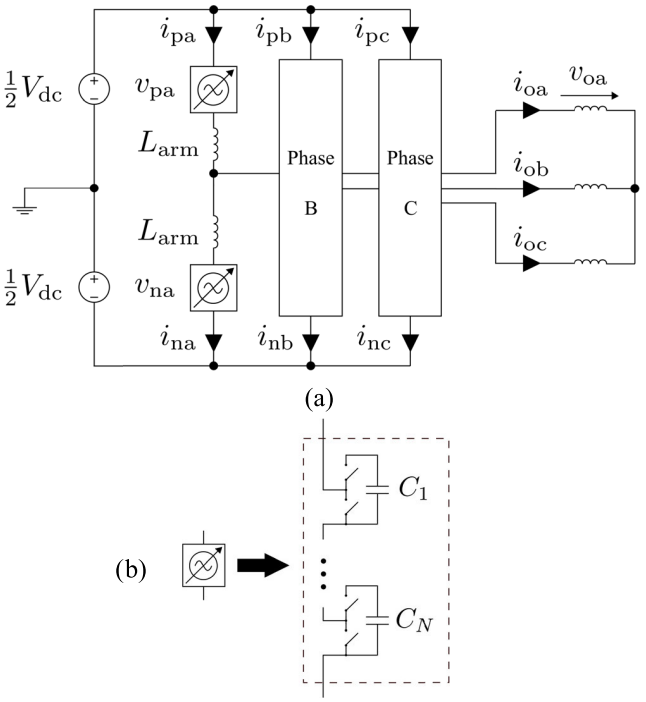

FIGURE 1. (a) Three-phase MMC and load. (b) Structure of one MMC arm.

The sinusoidal injection technique in [6] and [7] is considered in this work. Only Phase A is analyzed since the results can be conveniently extended to the other phases. The circulating current in Phase A is defined as

$$i_{za} = \frac{1}{2}\left(i_{pa} + i_{na}\right) \tag{1}$$

where i_{pa} and i_{na} are the upper and lower arm currents respectively in Phase A. For injection purposes, the common mode voltage v_{cm} and Phase A reference circulating current i^*_{za} are given by

$$v_{cm} = \hat{V}_{cm}\sin\left(2\pi f_{cm}t\right) \tag{2}$$

$$i^*_{za} = \frac{2V_{dc}}{\hat{V}_{cm}}\left(\frac{1}{4} - \frac{{v^*_{oa}}^2}{V^2_{dc}}\right) i_{oa}\sin\left(2\pi f_{cm}t\right) + \frac{v^*_{oa} i_{oa}}{V_{dc}} \tag{3}$$

where $\hat{V}_{cm}$ is the amplitude of injected common-mode voltage, and f_{cm} is the frequency of common-mode injection. In addition, v^*_{oa} and i_{oa} are the reference output (load) voltage and current of Phase A, respectively. Signals v^*_{oa} and i_{oa} are assumed to be sinusoids, whose frequency is called the output frequency f_o, and are phase-shifted by ϕ. That is,

$$v^*_{oa} = \hat{V}_o\sin\left(2\pi f_o t + \phi\right) \tag{4}$$

$$i_{oa} = \hat{I}_o\sin\left(2\pi f_o t\right) \tag{5}$$

If $f_{cm} \gg f_o$, then i^*_{za} contains components at multiple frequencies such as 0, $2f_o$ and f_{cm}.

The capacitor voltages in the upper arm can be derived by calculating the instantaneous power p_{pa}, which is equal to [7]

$$p_{pa} = f_1(t)\, V_{dc} i_{oa} \sin(2\pi f_{cm} t) + f_2(t)\, V_{dc} i_{oa} \cos(4\pi f_{cm} t) \tag{6}$$

Functions f_1 and f_2 include low-frequency content at f_o or close to it, and are given by

$$f_1(t) = \frac{V_{dc}}{\hat{V}_{cm}} \left(\frac{1}{4} - \frac{{v^*_{oa}}^2}{{V_{dc}}^2}\right) \left(1 - \frac{2v^*_{oa}}{V_{dc}}\right) - \frac{\hat{V}_{cm}}{2V_{dc}} - \frac{\hat{V}_{cm} v^*_{oa}}{V_{dc}^2} \tag{7}$$

$$f_2(t) = \frac{1}{4} - \frac{{v^*_{oa}}^2}{{V_{dc}}^2} \tag{8}$$

From (6), (7) and (8), it is clear that p_{pa} contain components in the vicinity of f_{cm} or $2f_{cm}$ if $f_{cm} \gg f_o$. The voltage fluctuations in the arm capacitors are thus sinusoids whose: 1) frequencies are equal to f_{cm} or $2f_{cm}$, and 2) amplitudes are inversely proportional to f_{cm}. As a result, it is desirable to increase f_{cm} as much as possible to reduce the voltage fluctuations or the capacitance size in the MMC submodules.

III. CIRCULATING CURRENT ERRORS

A. REASONS FOR CIRCULATING CURRENT ERRORS

Using high values for f_{cm} has its advantages as argued in Section II. However, there are many aspects to consider before selecting f_{cm}. In fact, if f_{cm} is very high then significant errors in the circulating currents may result. A typical block diagram for circulating current control is shown in Fig. 2, where the current is controlled by a proportional controller [7], [11]. Major reasons for current errors are explained below with the aid of Fig. 2:

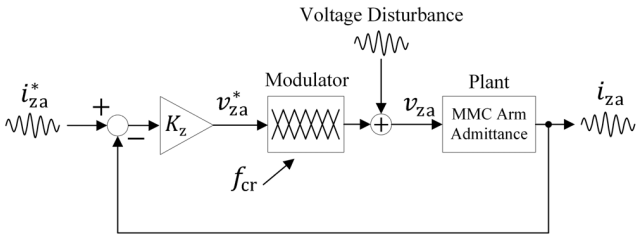

FIGURE 2. (a) Block diagram of circulating current control.

1) Since the circulating current contains components at many frequencies, it is easier to implement the control in the stationary frame of reference. However, doing so will inevitably cause phase delays between the reference and actual signals. The delay also increases when f_{cm} increases [17].
2) The carrier frequency f_{cr} determines the switching frequency of the power modules, and is normally chosen much higher than the frequency of modulated signals [18]. As f_{cm} increases and approaches f_{cr}, the current waveform gets more distorted leading to circulating current errors.

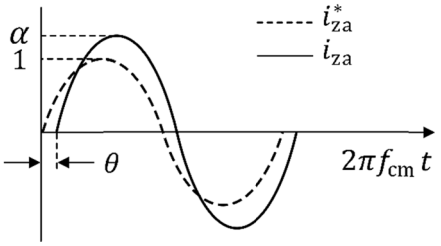

FIGURE 3. Normalized reference and actual circulating currents showing amplitude and phase deviations.

3) The circulating currents are controlled by inserting and bypassing the submodule capacitors. Furthermore, the circulating currents flow through the same capacitors, causing voltage fluctuations that act as a disturbance to the actual signal. The regulating voltage v^*_{za} is limited by the dc-link voltage. Thus, if the disturbance magnitude is large, then deviations between the reference and actual signals occur as v^*_{za} reaches the limit [17].

B. DEFINITION AND EFFECTS OF CIRCULATING CURRENT ERRORS

Based on the analysis in the previous subsection, circulating current components at f_{cm} are subjected to errors and distortion more than the other slower components at or near f_o. Thus, the focus is directed towards the deviations in the fast f_{cm} sinusoids in this research. The error in the circulating currents, in terms of amplitude and phase deviations has been investigated in the authors' earlier work [14]. The actual circulating current is assumed to be

$$i_{za} = \alpha \frac{2V_{dc}}{\hat{V}_{cm}} \left(\frac{1}{4} - \frac{{v^*_{oa}}^2}{{V_{dc}}^2}\right) i_{oa} \sin(2\pi f_{cm} t - \theta) + \frac{v^*_{oa} i_{oa}}{V_{dc}} \tag{9}$$

where α and θ, as illustrated in Fig. 3, represent respectively the amplitude and phase deviations between the idealized reference current in (3) and the actual current. When calculating the arm power using (9), there will be components at f_{cm} or $2f_{cm}$ as shown by (6). However, there will be an additional component independent of f_{cm}, which exists due to the circulating current error. This additional power component is referred to by p^{err}_{pa}, where "err" stands for error, and is given by [14]

$$p^{err}_{pa} = \frac{1}{4}(1 - \alpha \cos\theta)\, V_{dc} i_{oa} \tag{10}$$

In the case of perfect control performance without any error, $\alpha = 1$ and $\theta = 0$, and (10) evaluates to zero.

The existence of p^{err}_{pa} causes voltage fluctuations v^{err}_{cpa} in MMC capacitors. These fluctuations are governed by the differential equation [5], [15]

$$dv^{err}_{cpa}/dt = \frac{1}{4C}(1 - \alpha \cos\theta)\, i_{oa} \tag{11}$$

where C is the submodule capacitance. Both α and θ change continuously during operation [15], so obtaining an analytical

solution to (11) is not possible. However, it has been demonstrated that the frequency of v_{cpa}^{err} fluctuations is equal to f_o [15].

IV. PROPOSED TECHNIQUE FOR IMPROVED CAPACITOR VOLTAGE SUPPRESSION

A. SIMPLIFIED TECHNIQUE FOR CIRCULATING CURRENT ERROR COMPENSATION

The authors' initial technique to suppress v_{cpa}^{err} has been proposed in [14], where the circulating current reference in (3) is modified by two parameters α^* and θ^*, i.e.

$$i_{za}^{*}=\alpha^{*}\frac{2V_{dc}}{\hat{V}_{cm}}\left(\frac{1}{4}-\frac{{v_{oa}^{*}}^{2}}{{V_{dc}}^{2}}\right)i_{oa}\sin\left(2\pi f_{cm}t+\theta^{*}\right)+\frac{v_{oa}^{*}i_{oa}}{V_{dc}} \quad (12)$$

Referring to Fig. 3, the actual circulating current would be

$$i_{za}=\alpha^{*}\alpha\frac{2V_{dc}}{\hat{V}_{cm}}\left(\frac{1}{4}-\frac{{v_{oa}^{*}}^{2}}{{V_{dc}}^{2}}\right)i_{oa}\sin\left(2\pi f_{cm}t+\theta^{*}-\theta\right)+\frac{v_{oa}^{*}i_{oa}}{V_{dc}} \quad (13)$$

The circulating current in (13) would cause the undesired v_{cpa}^{err} fluctuations which, following the analysis in Section III, are equal to

$$dv_{cpa}^{err}/dt=\frac{1}{4C}\left[1-\alpha^{*}\alpha\cos\left(\theta^{*}-\theta\right)\right]i_{oa} \quad (14)$$

The goal from (14) is to eliminate v_{cpa}^{err} by choosing α^* and θ^* by trial-and-error such that the following criterion is met:

$$1-\alpha^{*}\alpha\cos\left(\theta^{*}-\theta\right)=0 \quad (15)$$

One problem with this approach is the large range of possible values for α^* and θ^*, a task that seems tedious for the control engineer. Another problem is, due to the continuous change of both α and θ in normal operation, it is not clear how (15) can be met with constant α^* and θ^* values. Therefore, the technique to suppress v_{cpa}^{err} is simplified by setting $\theta^* = 0$ in (15) and the objective becomes finding β^* such that

$$1-\beta^{*}\alpha\cos\theta\cong 0\Rightarrow\beta^{*}\cong\frac{1}{\alpha\cos\theta} \quad (16)$$

which leads to suppressing v_{cpa}^{err} fluctuations given by

$$dv_{cpa}^{err}/dt=\frac{1}{4C}\left[1-\beta^{*}\alpha\cos\theta\right]i_{oa} \quad (17)$$

To solve the problem of choosing β^* when α and θ exhibit variations, the average value of $\alpha\cos\theta$ is used to meet the compensation criterion (16) in this paper. Thus, assuming small variations of $\alpha\cos\theta$ around its average value

$$\alpha\cos\theta\cong\left(\alpha\cos\theta\right)_{avg} \quad (18)$$

then the compensation criterion (16) become

$$\beta^{*}\cong 1/\left(\alpha\cos\theta\right)_{avg} \quad (19)$$

Therefore, v_{cpa}^{err} can be suppressed by using (19) in (17):

$$dv_{cpa}^{err}/dt\cong\frac{1}{4C}\left[1-\beta^{*}\left(\alpha\cos\theta\right)_{avg}\right]i_{oa}\cong 0 \quad (20)$$

B. PROCEDURE FOR APPLYING PROPOSED TECHNIQUE

A two-steps procedure is suggested for applying the proposed injection technique to improve the capacitor voltage suppression. The reference circulating current is given by

$$i_{za}^{*}=\underbrace{\beta^{*}\frac{2\,V_{dc}}{\hat{V}_{cm}}\left(\frac{1}{4}-\frac{{v_{oa}^{*}}^{2}}{V_{dc}^{2}}\right)i_{oa}\sin\left(2\pi f_{cm}t\right)}_{\text{high -freq}}+\underbrace{\frac{v_{oa}^{*}I_{oa}}{V_{dc}}}_{\text{low}-\text{freq}} \quad (21)$$

A proportional controller for circulating current control is used as shown in Fig. 2. The procedure is as follows:

1) For a given set of $\hat{I}_o, f_o$ and f_{cm}, set $\beta^* = 1$ in (21) and choose a small value for the control gain K_z. Gradually increase K_z until minimal voltage fluctuations in the capacitor voltage are obtained.
2) Once minimal peak fluctuations have been reached in Step 1, slightly increase β^* to suppress the peak voltages further.

The above procedure can be repeated for several f_{cm} values until an optimal performance has been achieved. It is also suggested to have $\hat{I}_o$ as high as possible and f_o as low as possible, because the peak voltage fluctuation is directly proportional to $\hat{I}_o$ and is inversely proportional to f_o [5], [6].

C. VERIFICATION OF PROPOSED TECHNIQUE

The proposed technique is analyzed by: (i) observing the peak voltage fluctuations, (ii) calculating the amplitude of v_{cpa}^{err} using Fourier analysis, and (iii) computing the term $\beta^*\left(\alpha\cos\theta\right)_{avg}$. The method to perform the third task is described as follows: First, from the simulated waveforms of i_{oa} and dv_{cpa}^{err}/dt, the instantaneous value of the term $\beta^*\alpha\cos\theta$ is calculated using (17). The simulation model is built analytically, and all MMC state variables are calculated by integrating the vector field $\dot{x} = f(x, u, t)$ [16]. Thus, dv_{cpa}^{err}/dt is obtained from the readily-available dv_{cpa}^{err}/dt. A low-pass filter is used to remove switching transients and other high-frequency components as shown in Fig. 4.

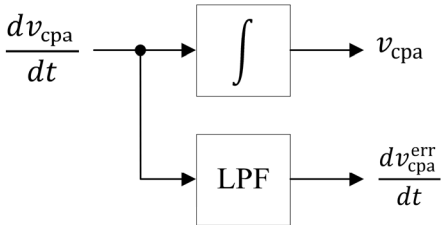

FIGURE 4. Obtaining dv_{cpa}^{err}/dt in simulation model.

When i_{oa} is close to zero, the effect of $\beta^*\alpha\cos\theta$ is negligible according to (17). That is,

$$i_{oa}\cong 0\Longrightarrow dv_{cpa}^{err}/dt\cong 0 \quad (22)$$

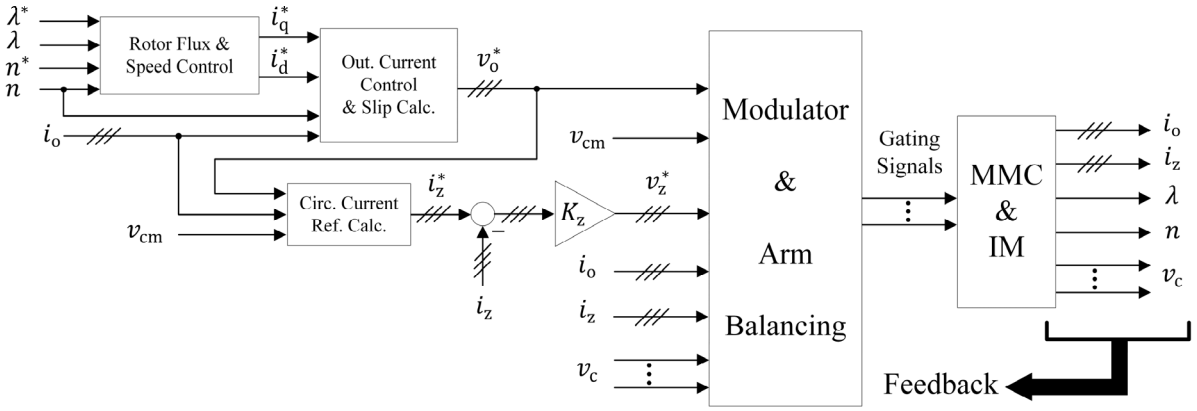

FIGURE 5. Simulation block diagram of MMC-based IM drive system.

TABLE 1. Simulation specifications and parameters.

MMC Specifications	Value	Unit
DC-link voltage	7000	V
Submodules per arm	6	
Nominal submodule voltage	1167	V
MMC Parameters		
Submodule capacitance	500	μF
Arm inductance	350	μH
Arm resistance	0.1	Ω
Induction Machine Parameters [20]		
Stator resistance	0.21	Ω
Rotor resistance	0.146	Ω
Stator, rotor leakage inductance	5.2	mH
Magnetizing inductance	155	mH
Control Parameters		
Carrier frequency	4	kHz
Sampling and control frequency	50	kHz
Peak common-mode voltage	1750	V

As a result, the instantaneous value of $\beta^*\alpha\cos\theta$ is calculated only when i_{oa} is greater than 10% of its amplitude:

$$\beta^*\alpha\cos\theta = \begin{cases} 1 - 4C\dfrac{dv_{cpa}^{err}/dt}{i_{oa}} & |i_{oa}| \geq 0.1\hat{I}_o \\ \text{don}'\text{t calculate} & |i_{oa}| < 0.1\hat{I}_o \end{cases} \quad (23)$$

Finally, $\beta^*\,(\alpha\cos\theta)_{avg}$ is calculated from all values computed in (23):

$$\beta^*\,(\alpha\cos\theta)_{avg} = \frac{\beta^*}{n}\sum_{k=1}^{n}(\alpha\cos\theta)\,[k] \quad (24)$$

For the technique to be effective in suppressing v_{cpa}^{err}, the $\beta^*\,(\alpha\cos\theta)_{avg}$ value should be close to 1 according to (20).

V. SIMULATION VERIFICATION

A system consisting of a seven-level MMC model, a field-oriented induction machine (IM) model and a control algorithm is developed and simulated in Matlab/Simulink. The

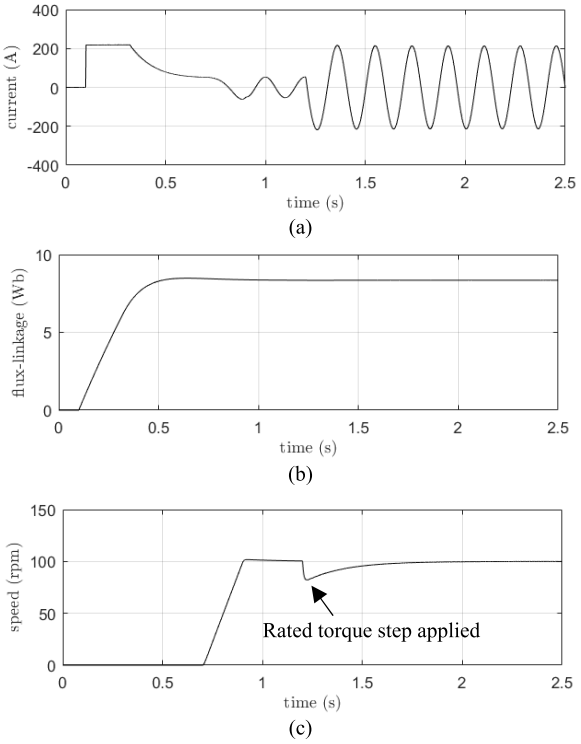

FIGURE 6. Simulation results showing machine startup and operation at low speed, (a) Output current in Phase A. (b) Rotor flux linkage. (c) Speed.

block diagram of the simulated system structure is shown in Fig. 5. The control cycle starts by determining the required output current references. Then, the output current regulation and slip calculation tasks are performed, and the required three-phase output voltages v_o^* are calculated. After the v_o^* vector is determined, the circulating current reference i_z^* for each phase is computed using (21). The reference voltages v_o^* and v_z^* for each phase, along with the common-mode voltage v_{cm} selected by (2), determine the required number of submodules in each arm through modulation with six phase-shifted carrier signals [19]. The gating signals for each

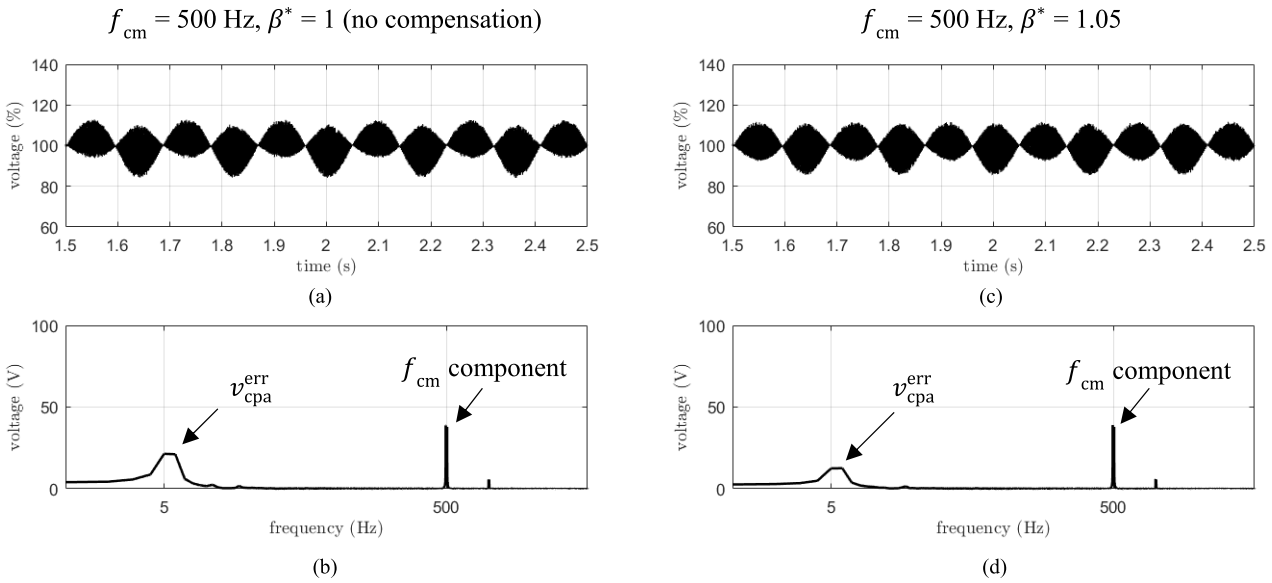

FIGURE 7. Simulation results for $f_{cm} = 500$ Hz, and two cases of β^*: 1 (no compensation) and 1.05. (a) One capacitor voltage in the upper arm of Phase A for $\beta^* = 1$. (b) Fourier analysis of capacitor voltage for $\beta^* = 1$. (d) One capacitor voltage in the upper arm of Phase A for $\beta^* = 1.05$. (b) Fourier analysis of capacitor voltage for $\beta^* = 1.05$.

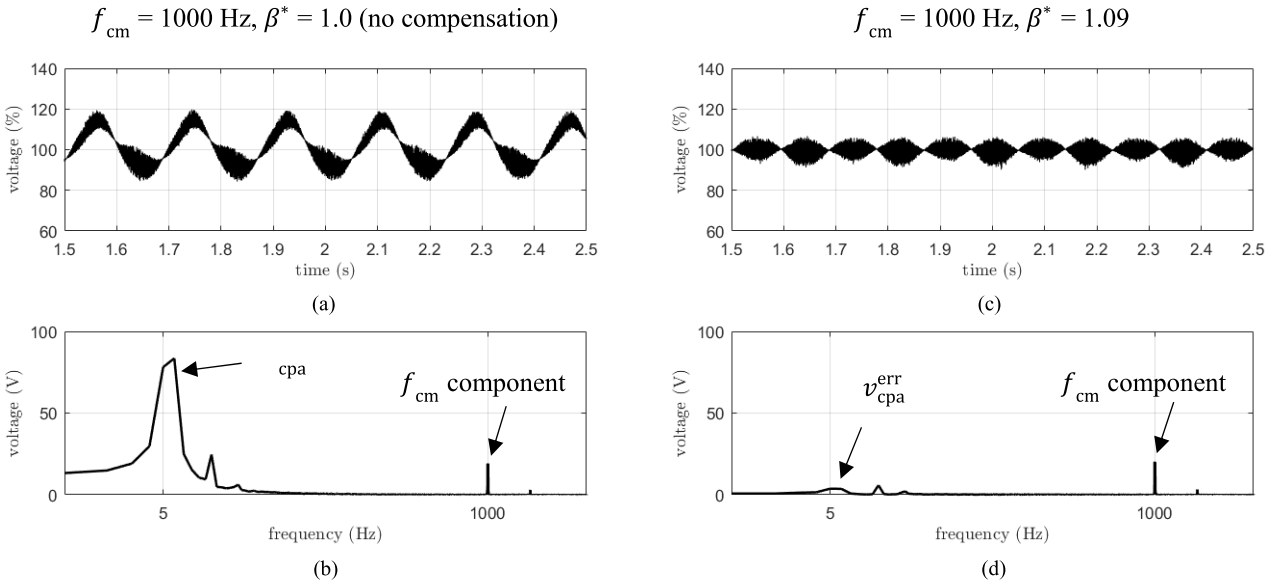

FIGURE 8. Simulation results for $f_{cm} = 1000$ Hz, and two cases of β^*: 1 (no compensation) and 1.03. (a) One capacitor voltage in the upper arm of Phase A for $\beta^* = 1$. (b) Fourier analysis of capacitor voltage for $\beta^* = 1$. (c) One capacitor voltage in the upper arm of Phase A for $\beta^* = 1.09$. (d) Fourier analysis of capacitor voltage for $\beta^* = 1.09$.

submodule are applied to the MMC model. The system specifications and parameters are given in Table 1.

The drive system is simulated for 2.5 seconds. The output current of Phase A, rotor flux-linkage and speed are shown in Fig. 6. Initially the MMC capacitors are charged to the nominal voltage and the IM is at standstill. At $t = 0.1$ s the IM is magnetized with the rated flux linkage of 8.35 Wb, and at $t = 0.7$ s the speed is ramped up to 100 rpm, which is equivalent to 5 Hz electrical. A rated torque step of 7490 Nm is applied at $t = 1.2$ s, and the system is stabilized at $t = 1.5$ s. The rated flux-linkage and torque values result in rated output (stator) currents of 150 A rms.

The capacitor voltages are analyzed once the system is at steady-state at $t = 1.5$ s. Two values for f_{cm} are chosen: 500 and 1000 Hz, and the effects before and after applying the proposed technique are analyzed. Furthermore, the control gain K_z in each f_{cm} case is chosen as described in the proposed procedure in Section IV.

The results for $f_{cm} = 500$ Hz are shown in Fig. 7. On the left column, a capacitor voltage v_{cpa}, and its Fourier analysis

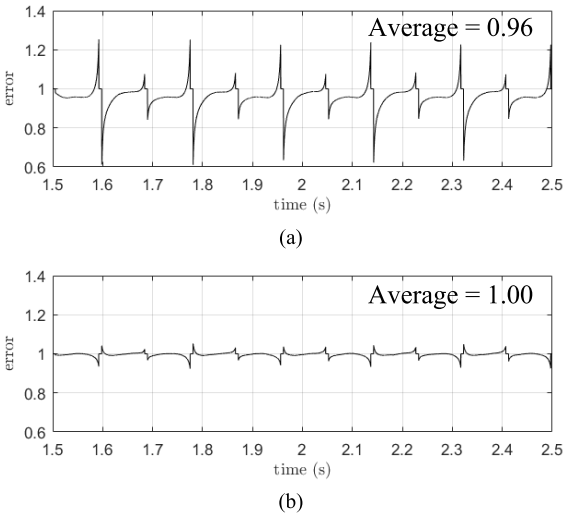

FIGURE 9. Computed term $\beta^*\alpha\cos\theta$ using $f_{cm} = 1000$ Hz and (a) $\beta^* = 1$. (b) $\beta^* = 1.09$.

are shown for the case not utilizing the proposed technique (i.e. $\beta^* = 1$). Note that the capacitor voltage is shown as a percentage of the nominal value, and that the Fourier analysis does not include the nominal value for better visibility. The peak fluctuation of v_{cpa} is +13% in Fig. 7 (a), and it includes major components at f_o and f_{cm}. The voltage component at f_o is indeed v_{cpa}^{err} derived in (17) and exists due to the circulating current error. To suppress the voltage fluctuations further, the proposed technique is applied using $\beta^* = 1.05$, and the results are shown in the right column of Fig. 7. Although v_{cpa}^{err} got reduced by applying β^*, the overall reduction in the voltage fluctuations is not substantial because the f_{cm} voltage component is large when $f_{cm} = 500$ Hz. Only a 1% drop in the voltage fluctuations is obtained in this case.

The same set of results are obtained for $f_{cm} = 1000$ Hz and are shown in Fig. 8. Without compensation, the v_{cpa}^{err} is very large as shown in Fig. 8 (b), and much larger than calculated in Fig. 7 (b). Furthermore, the voltage fluctuates to +20% of its nominal in Fig. 8 (a). After applying the proposed technique using $\beta^* = 1.09$, the suppression of voltage fluctuations is significantly enhanced, where the peak fluctuation is reduced from +20% to 7%. The reason behind this reduction is the suppression of v_{cpa}^{err}, whose amplitude went down from 84 V to 4 V.

Further close-up examination is presented for the $f_{cm} = 1000$ Hz case by analyzing the term $\beta^*\alpha\cos\theta$ and its average value $\beta^*(\alpha\cos\theta)_{avg}$. The instantaneous variations of $\beta^*\alpha\cos\theta$ are shown in Fig. 9 for $\beta^* = 1$ and $\beta^* = 1.09$. Without applying the technique ($\beta^* = 1$), the value $\beta^*(\alpha\cos\theta)_{avg}$ is 0.95. However, using the technique with $\beta^* = 1.09$ brings $\beta^*(\alpha\cos\theta)_{avg}$ to a value of 1, which is the key to eliminate v_{cpa}^{err} in (20) and enhance the suppression of the voltage fluctuations in the MMC capacitors.

A summary of simulation results given in Table 2 shows when f_{cm} is increased from 500 Hz to 1500 Hz the voltage fluctuations increase from 13% to 22 % without compensation. On the other hand, when the proposed technique is applied, the peak voltage fluctuations, as opposed to the conventional technique, decreases from 12% to 6%, under a similar increase in the frequency. Thus, a significant advantage of the proposed technique is shown. It is also worth mentioning that the carrier frequency is maintained constant in all cases shown in Table 2. Therefore, there is no big change in the switching frequency.

VI. EXPERIMENTAL RESULTS

The laboratory investigation to validate the proposed technique has been conducted on a three-level ($N = 2$) MMC [21] feeding a three-phase inductive load. A Texas Instruments TMS320F28379D digital signal processor (DSP) and an Altera Cyclone IV field-programmable gate array (FPGA) are used for control and protection of the overall system.

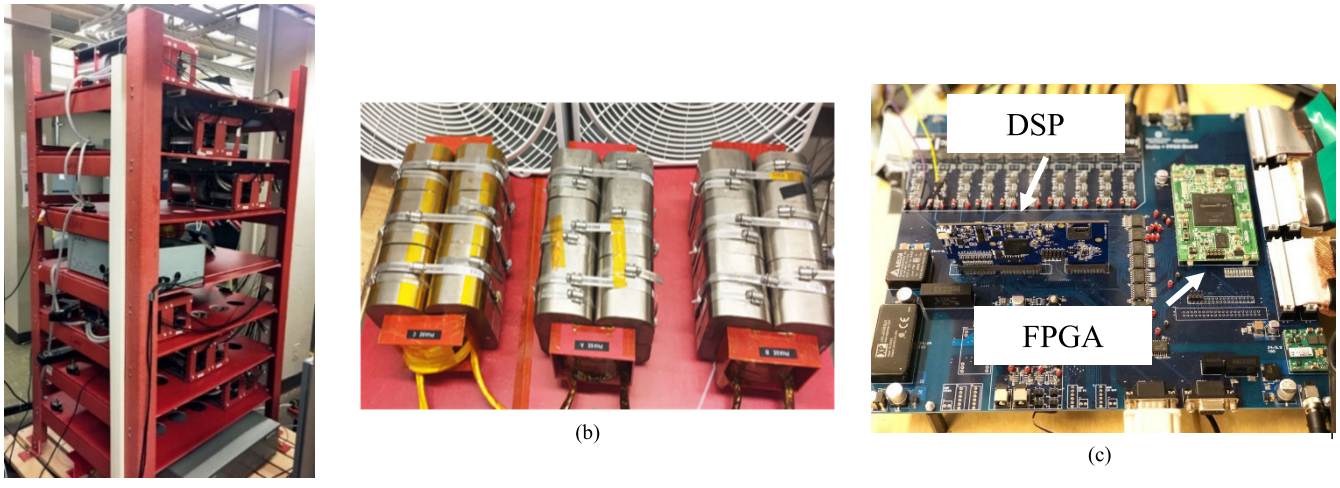

FIGURE 10. Experimental testing setup. (a) MMC with 12 submodules. (b) Three-phase inductive load. (c) DSP and FPGA boards.

TABLE 2. Summary of simulation results.

		Without compensation ($\beta^* = 1$)		With compensation		
f_{cm} (Hz)	K_z	Peak voltage fluctuation	v_{cpa}^{err} amplitude (V)	β^*	Peak voltage fluctuation	v_{cpa}^{err} amplitude (V)
500	1	+13%	21	1.05	+12%	13
1000	5	+20%	84	1.09	+7%	4
1500	8	+22%	97	1.08	+6%	5

TABLE 3. Specifications and parameters of experinemtal setup.

MMC Specifications	Value	Unit
DC-link voltage	600	V
Submodules per arm	2	
Nominal submodule voltage	300	V
MMC Parameters		
Submodule capacitance	620	μF
Arm inductance	114	μH
Load inductance	1.7	mH
Control Parameters		
Carrier frequency	4	kHz
Sampling and control frequency	50	kHz
Peak common-mode voltage	210	V

The hardware implementation is shown in Fig. 10, and the system specification and parameters are given in Table 3. Experimental results have been obtained for $f_{cm} = 200$, and 1000 Hz. The former is the highest choice for f_{cm} found in literature, while the latter results in large circulating current error that can be compensated with the presented technique. In both cases, the output current amplitude $\hat{I}_o$ is 50 A, and the output frequency f_o is 5 Hz.

Experimental investigation is performed with two objectives. Firstly, the effect of increasing frequency is analyzed by operating the system at $f_{cm} = 200$ and 1000 Hz without any compensation. Secondly, the proposed technique is applied at 1000 Hz to show its effectiveness for suppressing the voltage fluctuations.

The case using $f_{cm} = 200$ Hz is shown in Fig. 11. Shown are one capacitor voltage in the upper arm and its Fourier analysis, upper arm current and output current without applying the proposed technique, i.e. $\beta^* = 1$. All measurements are made on one phase. The control gain K_z is chosen such that peak voltage fluctuation is minimized. The peak voltage fluctuation is 19% above its nominal value as illustrated in subplot (a) of Fig. 11. A look at the frequency content reveals two major components. The first one is at f_o (5 Hz), which is v_{cpa}^{err} derived in (11), and the second is at f_{cm} (200 Hz). If v_{cpa}^{err} was to be suppressed, then the overall gain would not be substantial since the f_{cm} component is also large.

Experimental results for $f_{cm} = 1000$ Hz, also without applying the proposed technique, are shown in Fig. 12. The peak voltage fluctuation in Fig. 12 (a) is +22%, which has not changed much as compared to Fig. 11 (a). However, the magnitudes of individual voltage components at f_o and f_{cm} changed as the Fourier analysis in Fig. 12 (b) illustrates. The magnitude of v_{cpa}^{err} increased when f_{cm} went from 200 to

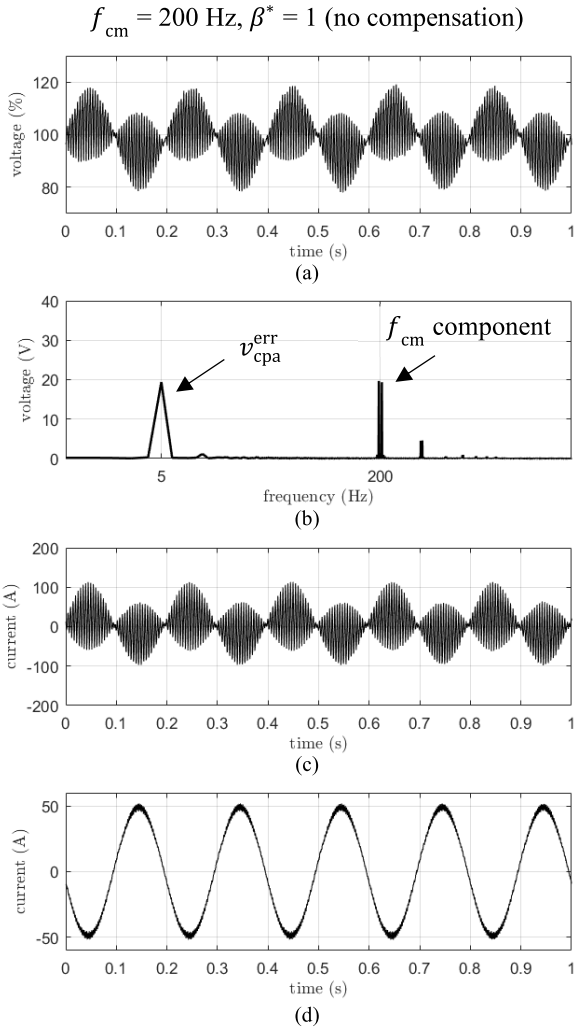

FIGURE 11. Experimental results for $f_{cm} = 200$ Hz and $\beta^* = 1$ (no compensation) (a) One capacitor voltage in upper arm of Phase A (b) Fourier analysis of capacitor voltage (c) Phase A upper arm current (d) Phase A output current.

1000 Hz due to the increase in circulating current error (see Section III). On the other hand, the voltage component at f_{cm} is substantially reduced as f_{cm} is increased from 200 to 1000 Hz. From Fig. 12 (b) it is clear when the v_{cpa}^{err} is suppressed the overall voltage fluctuations are significantly reduced.

The effectiveness of proposed technique is validated at 1000 Hz with $\beta^* = 1.5$, and the results are shown in Fig. 13. The v_{cpa}^{err} component is suppressed, and the voltage is more stabilized. Specifically, the peak voltage fluctuation is reduced to +8% as shown in Fig. 13 (a), and this substantial reduction is attributed to the elimination of v_{cpa}^{err} shown in Fig. 13 (b).

The peak voltage fluctuations in case of 200 and 1000 Hz without compensation ($\beta^* = 1$) are observed to be 19% and 22% respectively. When the proposed technique with $\beta^* = 1.5$ is applied for $f_{cm} = 1000$ Hz, the peak voltage fluctuations are reduced from 22% to 8%, a significant reduction of more than 63.6%, showing the effectiveness of proposed technique.

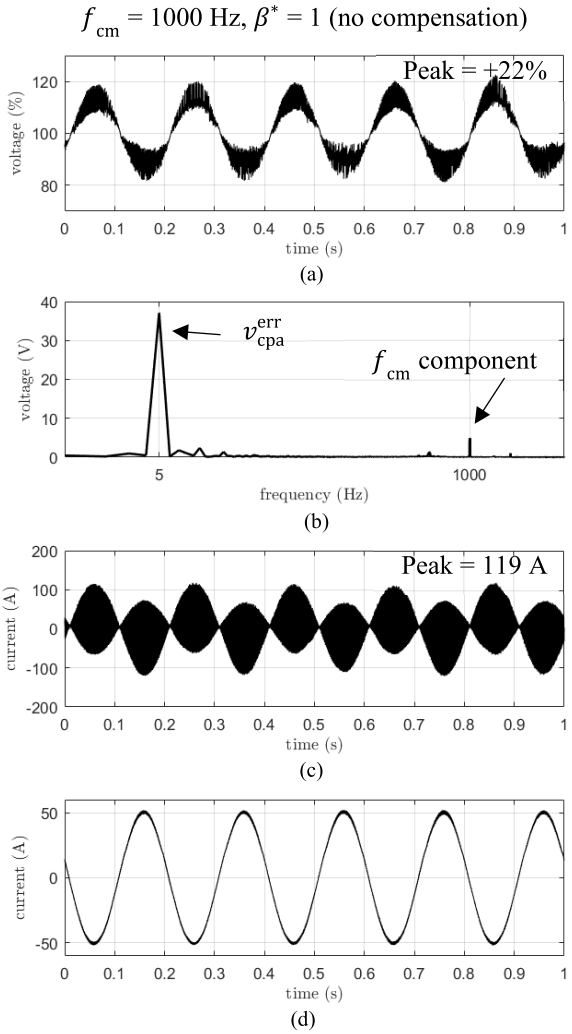

FIGURE 12. Experimental results for f_{cm} = 1000 Hz and β^* = 1 (no compensation) (a) One capacitor voltage in upper arm of Phase A (b) Fourier analysis of capacitor voltage (c) Phase A upper arm current (d) Phase A output current.

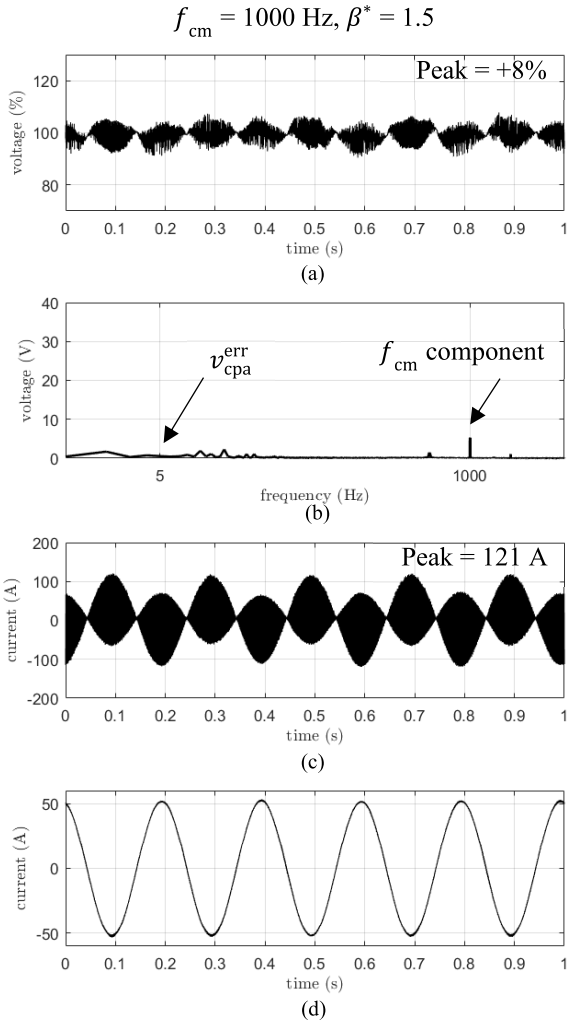

FIGURE 13. Experimental results for f_{cm} = 1000 Hz and β^* = 1.5 (no compensation) (a) One capacitor voltage in upper arm of Phase A (b) Fourier analysis of capacitor voltage (c) Phase A upper arm current (d) Phase A output current.

The experimental results in Fig. 13 also show an increase in arm currents by 2 A from 1000 Hz injection to enhanced 1000 Hz injection. The increase can be understood by realizing a β^* greater than one increases the circulating currents and, consequently, the arm currents. However, the current increase is insignificant when weighted against the reduction in capacitor voltage fluctuations. In addition, one carrier frequency is utilized in all the cases. Thus, the actual switching frequency of semiconductor devices does not change. Another aspect to point out is the noticeable improvement in the output current quality. That is, the output current becomes smoother when increasing f_{cm} and applying the proposed technique (compare Fig. 11 (d) and Fig. 13 (d)).

VII. CONCLUSION

This paper has proposed a new technique for the suppression of capacitor voltages in MMCs operated at low output frequency. The technique suggests using very high common-mode frequencies while simultaneously compensating the errors associated with such frequencies. The problem and proposed solution has been analyzed mathematically. Both the simulation and experimental results validated the effectiveness of the presented technique. The experimental results demonstrated that peak voltage fluctuations are reduced from 22% to 8%, i.e. 63.6 % reduction, by applying the technique proposed in this work. The resulting reduction in the voltage fluctuations allows using smaller capacitor size and, hence, increases the overall energy density.

ACKNOWLEDGMENT

Publication in IEEE Access was supported by the Open Access Program from the American University of Sharjah. This paper represents the opinions of the authors and does not mean to represent the position or opinions of the American University of Sharjah.

REFERENCES

[1] R. Marquardt, A. Lesnicar, and J. Hildinger, "Modulares Stromrichterkonzept fur Netzkupplungsanwendungen bei hohen Spannungen," presented at the ETG-Fachtagungen, Bad Nauheim, Germany, 2002.

[2] A. Lesnicar and R. Marquardt, "An innovative modular multilevel converter topology suitable for a wide power range," in *Proc. IEEE Bologna Power Tech Conf.*, vol. 3. Bologna, Italy, Jun. 2003, p. 6.
[3] M. A. Perez, S. Bernet, J. Rodriguez, S. Kouro, and R. Lizana, "Circuit topologies, modeling, control schemes, and applications of modular multilevel converters," *IEEE Trans. Power Electron.*, vol. 30, no. 1, pp. 4–17, Jan. 2015.
[4] S. Debnath, J. Qin, B. Bahrani, M. Saeedifard, and P. Barbosa, "Operation, control, and applications of the modular multilevel converter: A review," *IEEE Trans. Power Electron.*, vol. 30, no. 1, pp. 37–53, Jan. 2015.
[5] M. Hagiwara, K. Nishimura, and H. Akagi, "A medium-voltage motor drive with a modular multilevel PWM inverter," *IEEE Trans. Power Electron.*, vol. 25, no. 7, pp. 1786–1799, Jul. 2010.
[6] A. J. Korn, M. Winkelnkemper, and P. Steimer, "Low output frequency operation of the modular multi-level converter," in *Proc. IEEE Energy Convers. Congr. Exposit.*, Atlanta, GA, USA, Sep. 2010, pp. 3993–3997.
[7] M. Hagiwara, I. Hasegawa, and H. Akagi, "Start-up and low-speed operation of an electric motor driven by a modular multilevel cascade inverter," *IEEE Trans. Ind. Appl.*, vol. 49, no. 4, pp. 1556–1565, Jul. 2013.
[8] A. Antonopoulos, L. Angquist, S. Norrga, K. Ilves, L. Harnefors, and H.-P. Nee, "Modular multilevel converter AC motor drives with constant torque from zero to nominal speed," *IEEE Trans. Ind. Appl.*, vol. 50, no. 3, pp. 1982–1993, May 2014.
[9] J. Kolb, F. Kammerer, M. Gommeringer, and M. Braun, "Cascaded control system of the modular multilevel converter for feeding variable-speed drives," *IEEE Trans. Power Electron.*, vol. 30, no. 1, pp. 349–357, Jan. 2015.
[10] J.-J. Jung, H.-J. Lee, and S.-K. Sul, "Control strategy for improved dynamic performance of variable-speed drives with modular multilevel converter," *IEEE J. Emerg. Sel. Topics Power Electron.*, vol. 3, no. 2, pp. 371–380, Jun. 2015.
[11] S. Debnath, J. Qin, and M. Saeedifard, "Control and stability analysis of modular multilevel converter under low-frequency operation," *IEEE Trans. Ind. Electron.*, vol. 62, no. 9, pp. 5329–5339, Sep. 2015.
[12] B. Li, S. Zhou, D. Xu, R. Yang, D. Xu, C. Buccella, and C. Cecati, "An improved circulating current injection method for modular multilevel converters in variable-speed drives," *IEEE Trans. Ind. Electron.*, vol. 63, no. 11, pp. 7215–7225, Nov. 2016.
[13] Z. Wang, J. Chen, K. Liao, J. Xiong, and K. Zhang, "Review on low-frequency ripple suppression methods for MMCs for medium-voltage drive applications," *IET Power Electron.*, vol. 11, no. 15, pp. 2403–2414, Dec. 2018.
[14] M. Al Sabbagh, J. Pan, Z. Ke, R. Na, and L. Xu, "Error effects of compensation circulating current of modular multilevel converters in low frequency motor drive operation," in *Proc. 20th Eur. Conf. Power Electron. Appl.*, Riga, Latvia, Sep. 2018, p. 1.
[15] M. Al Sabbagh, J. Pan, Z. Ke, and L. Xu, "Investigation and compensation of circulating current errors in low frequency operation of modular multilevel converters," in *Proc. IEEE Energy Convers. Congr. Exposit. (ECCE)*, Portland, OR, USA, Sep. 2018, pp. 6054–6061.
[16] S. Debnath and M. Saeedifard, "Simulation-based gradient-descent optimization of modular multilevel converter controller parameters," *IEEE Trans. Ind. Electron.*, vol. 63, no. 1, pp. 102–112, Jan. 2016.
[17] R. C. Dorf and R. H. Bishop, *Modern Control Systems*, 9th ed. Upper Saddle River, NJ, USA: Prentice-Hall, 2001.
[18] M. P. Kazmierkowski and L. Malesani, "Current control techniques for three-phase voltage-source PWM converters: A survey," *IEEE Trans. Ind. Electron.*, vol. 45, no. 5, pp. 691–703, Oct. 1998.
[19] G. S. Konstantinou and V. G. Agelidis, "Performance evaluation of half-bridge cascaded multilevel converters operated with multicarrier sinusoidal PWM techniques," in *Proc. 4th IEEE Conf. Ind. Electron. Appl.*, May 2009, pp. 3399–3404.
[20] H. Gao, B. Wu, D. Xu, M. Pande, and R. P. Aguilera, "Common-Mode-Voltage-Reduced model-predictive control scheme for Current-Source-Converter-Fed induction motor drives," *IEEE Trans. Power Electron.*, vol. 32, no. 6, pp. 4891–4904, Jun. 2017.
[21] H. Li, K. Potty, Z. Ke, J. Pan, Y. Chen, F. Zhang, M. A. Sabbagh, W. Perdikakis, G. Li, X. Ye, R. Na, J. Zhang, L. Xu, and J. Wang, "Hardware design of a 1.7 kV SiC MOSFET based MMC for medium voltage motor drives," in *Proc. IEEE Appl. Power Electron. Conf. Exposit. (APEC)*, San Antonio, TX, USA, Mar. 2018, pp. 1649–1655.

MUNEER AL SABBAGH (Member, IEEE) received the B.S. degree from the American University of Sharjah, Sharjah, UAE, the M.S. degree from RWTH Aachen University, Aachen, Germany, and the Ph.D. degree from The Ohio State University, Columbus, OH, USA, in 2009, 2012, and 2019, respectively. From 2012 to 2013, he was with ABB, Turgi, Switzerland, as an Research and Development Control Software Engineer. His research interests include the control of electric drives and power converters.

HABIBUR REHMAN (Member, IEEE) received the B.Sc. degree in electrical engineering from the University of Engineering and Technology at Lahore, Lahore, Pakistan, in 1990, and the M.S. and Ph.D. degrees in electrical engineering from The Ohio State University, Columbus, OH, USA, in 1995 and 2001, respectively.

He has a wide experience in the areas of power electronics and motor drives in both industry and academia. From 1998 to 1999, he was a Design Engineer with Ecostar Electric Drive Systems and Ford Research Laboratory, where he was a member of the Electric, Hybrid, and Fuel Cell Vehicle Development Programs. From 2001 to 2006, he was with the Department of Electrical Engineering, United Arab Emirates (UAE) University, Al Ain, UAE, as an Assistant Professor. In 2006, he joined the Department of Electrical Engineering, American University of Sharjah, where he is currently an Associate Professor. His primary research interests are in the areas of power electronics and their application to power systems, adjustable-speed drives, and alternative energy vehicles. He was a recipient of the Best Teacher Award (2002–2003) from the College of Engineering, UAE University.

JIANYU PAN (Member, IEEE) received the B.S. and M.S. degrees from Chongqing University, Chongqing, China, in 2011 and 2014, respectively, and the Ph.D. degree from The Ohio State University, Columbus, OH, USA, in 2019, all in electrical engineering. He is currently an Assistant Professor with the School of Electrical Engineering, Chongqing University. His research interests include power converters, electric machine control, wide-bandgap semiconductor applications, and high-voltage engineering.

LONGYA XU (Fellow, IEEE) received the M.S. and Ph.D. degrees from the University of Wisconsin-Madison, in 1986 and 1990, respectively, both in electrical engineering.

He is currently a Professor and Director of the Center for High Performance Power Electronics, The Ohio State University. His research interests include design and control of novel electric machines, power electronics, and digital technology for electrified transportation and renewable energy systems. He has received the several IEEE prestigious awards, including the First Prize Paper Award 1992 from the Industry Drive Committee IEEE/IAS, the Best Transaction Paper Award 2013 and Outstanding Achievement Award 2014, and the Highest Society Award from the IEEE Industry Application Society. He is a recipient of the Nikola Tesla Award for his outstanding contributions to the generation and utilization of electric power. He has served as the Chairperson of Electric Machine Committee of the IEEE/IAS and an Associate Editor of the IEEE Transactions on Power Electronics over the past two decades. He was a member-at-large on the IEEE/IAS Executive Board and the Conference Co-Chair for the IEEE Transportation Electrification Conference and Expo, AP 2014, 2016, and 2019, respectively.